1995

Mathematical Modeling of a Nickel-Cadmium Cell: Proton Diffusion in the Nickel Electrode

Pauline De Vidts
Texas A & M University - College Station

Ralph E. White
University of South Carolina - Columbia, white@cec.sc.edu

Publication Info

Journal of the Electrochemical Society, 1995, pages 1509-1519.

Mathematical Modeling of a Nickel-Cadmium Cell: Proton Diffusion in the Nickel Electrode

Pauline De Vidts*

Department of Chemical Engineering, Texas A&M University, College Station, Texas 77843

Ralph E. White**

Department of Chemical Engineering, University of South Carolina, Columbia, South Carolina 29208

ABSTRACT

In this paper we present a mathematical model of a sealed nickel-cadmium cell that includes proton diffusion and ohmic drop through the active material in the nickel electrode. The model is used to calculate sensitivity coefficients for various parameters in the model. These calculations show that the discharge voltage of the cell is affected mostly by the kinetics of the nickel reaction. Toward the end of discharge, proton diffusion also becomes important, because the proton diffusion process affects the active material utilization significantly. During charge, the cell voltage is mainly affected by the kinetics of the nickel reaction until the oxygen evolution reaction begins, after which time the kinetics of the oxygen evolution has the largest effect. The oxygen evolution reaction is also the most influencing factor on the actual charge uptake of the cell by the end of a charge operation (charge efficiency). Compared to the rates of reaction and proton diffusion, the ohmic drop in the active material of the nickel electrode and the mass transport and ohmic drop in the electrolyte have negligible effect on the behavior of the cell studied here.

Introduction

Many researchers and manufacturers are interested in the charge and discharge performance of the nickel-cadmium battery (Ni-Cd). It is well known that the battery performance is the result of complex chemical and physical phenomena[1-3] that take place inside the battery. A mathmatical model of an Ni-Cd cell can be used to help understand these phenomena.

Fan and White[4,5] developed a one-dimensional (1D) model for the charge and discharge operations of a nickel-cadmium cell, which is similar to a model for a nickel-zinc cell presented by Choi and Yao.[6] Fan and White[4,5] included the oxygen reaction in both electrodes and used a non-Nernst expression for the equilibrium potential in the nickel electrode. They used this model to predict the experimental observation that the oxygen reaction is important toward the end of charge and during overcharge because it reduces the utilization of the active material. For low rates of discharge, Fan and White[4,5] found that the model predictions were in fair agreement with the experimental data for moderate rates of discharge. However, for high discharge rates the predictions deviated from the experimental observations. Specifically, their model does not predict the decrease of active material utilization as the rate of discharge is increased, as discussed by Timmerman *et al.*[7] Contrary to Choi and Yao,[6] Fan and White[4,5] found that the mass transport in the electrolyte phase has little effect on the electrode behavior. They concluded that the charge and discharge behavior of the nickel-cadmium cell is under kinetic control.

Some researchers[8-11] have proposed that the proton diffusion in the active material of the nickel electrode controls the performance of the cell. Bouet *et al.*[12] developed a pseudo 2D model for the discharge operation of the nickel electrode that incorporates this proton diffusion process. Their model simulations are in excellent agreement with their experimental data. The nickel electrode discharge predictions obtained by Bouet *et al.*[12] exhibit a significant improvement in simulating experimental observations over those from models that do not include the proton diffusion process.[4-6,13,14] Their simulations show that the active material utilization is affected by the proton diffusion process. Mao *et al.*[15] reached the same conclusion with a model for the discharge of a nickel-hydrogen cell that includes the proton diffusion in the nickel electrode.

Some studies[8,11] indicate that the ohmic drop through the active material of the nickel electrode also may affect the behavior of the electrode. Experimental results reported by Zimmerman and Effa[11] showed that the proton diffusion process controls most of the discharge of the nickel electrode. They also found that, as the electrode is being discharged, the conductivity of the active material decreases until the proton diffusion no longer controls the discharge and mixed control becomes evident. Further discharge results in the formation of a semiconductor layer that controls the last portion of the discharge.

Proton diffusion and the ohmic drop in the active material of the nickel electrode have been identified as possible important factors in the behavior of the nickel electrode. However, these factors have not been included in a model for the nickel-cadmium battery. Our purpose here is to present a mathematical model of a sealed nickel-cadmium cell that includes proton diffusion and ohmic drop through the active material in the nickel electrode and to evaluate the effect of these phenomena on the predicted behavior of the cell during charge and discharge. This was done by conducting a sensitivity analysis of various model parameters on the voltage of the cell over time and the charge utilization for discharge and charge operation. We found that the kinetic parameters of the nickel electrode reaction have the largest effect on the predicted cell voltage during discharge. Also, the proton diffusion coefficient becomes important toward the end of discharge because it has the largest effect on the active material utilization. During charge, the kinetic parameters of the main reactions of both electrodes are the most important parameters until the oxygen evolution reaction begins on the nickel electrode. Then the kinetic parameters for oxygen evolution become the most important parameters affecting the cell voltage and the actual charge uptake of the cell by the end of a charge operation. The parameters involved in the mass transfer of electrolyte, the ohmic drop in the electrolyte, and the ohmic drop in the active material of the nickel electrode have a negligible effect on the predicted cell voltage and charge utilization in the cell.

The model presented here can be used to predict the performance of the Ni-Cd cell during charge and discharge. Therefore, it can assist battery designers and engineers in studying the effect of various design parameters on battery performance.

Model Development

Figure 1 shows a schematic diagram of the cross-sectional view of the nickel-cadmium cell and the idealization

* Electrochemical Society Student Member.
** Electrochemical Society Active Member.

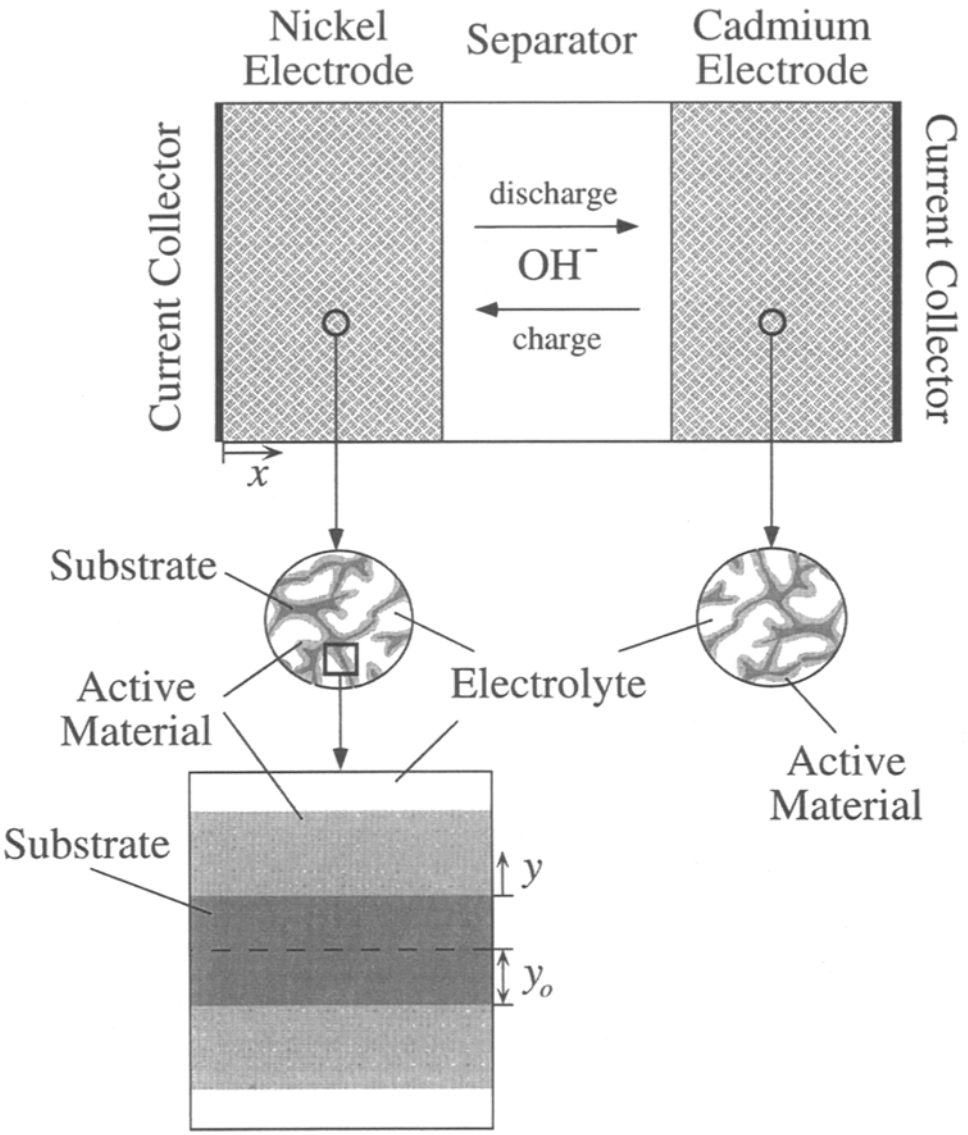

Fig. 1. A schematic diagram of the representation of the nickel-cadmium cell in the model.

of the cell as it is represented in the mathematical model. The nickel-cadmium cell consists of three regions: the positive electrode (porous nickel oxyhydroxide), the separator, and the negative electrode (porous cadmium). The electrolyte is a concentrated KOH aqueous solution. The electrochemical reactions included in the model are

Positive (nickel) electrode

$$\mathrm{NiOOH + H_2O + } e^- \underset{\text{charge}}{\overset{\text{discharge}}{\rightleftharpoons}} \mathrm{Ni(OH)_2 + OH^-} \quad [1]$$

$$\frac{1}{2}\,\mathrm{O_2 + H_2O + } 2e^- \underset{\text{charge}}{\overset{\text{discharge}}{\rightleftharpoons}} \mathrm{2\ OH^-} \quad [2]$$

Negative (cadmium) electrode

$$\mathrm{Cd + 2\ OH^-} \underset{\text{charge}}{\overset{\text{discharge}}{\rightleftharpoons}} \mathrm{Cd(OH)_2} + 2e^- \quad [3]$$

$$\mathrm{2\ OH^-} \underset{\text{charge}}{\overset{\text{discharge}}{\rightleftharpoons}} \frac{1}{2}\,\mathrm{O_2 + H_2O} + 2e^- \quad [4]$$

In the following paragraphs we present the model equations. The equations are formulated separately for the nickel electrode, the separator, and the cadmium electrode.

Positive electrode.—We use a pseudo-2D approach to treat the mass transfer and ohmic losses in the nickel electrode. This representation is the same as the one we use in the model for a nickel/hydrogen cell.[15] In this pseudo-2D model, the x dimension is defined across the electrode, and the pseudo-y dimension is defined inside the layer of active material from the nickel substrate to the interface with the electrolyte, as shown in Fig. 1. In our representation of the nickel electrode, the current collector (nickel screen) is placed in the center of the electrode, which corresponds to $x = 0$. Thus, the total thickness of the electrode is $2l_1$. The surface of the nickel electrode which is in contact with the separator corresponds to $x = l_1$. The governing equations were derived using the theory for concentrated electrolytes[16] and the theory for porous electrodes.[17]

Equations in the x-direction.—The equations are written for four dependent variables: the electrolyte concentration, c; the oxygen concentration, c_{O_2}; the potential in the liquid phase, ϕ_2; and the current density in the liquid phase, i_2. The equations that describe the behavior of the positive electrode are

Material balance on electrolyte (KOH)

$$\epsilon_1 \frac{\partial c}{\partial t} = \epsilon_1^{\gamma_1} \frac{\partial}{\partial x}\left(D_{\mathrm{OH}} \frac{\partial c}{\partial x}\right) + \frac{(t_-^\circ - 1)}{F} \frac{\partial i_2}{\partial x} \quad [5]$$

Material balance on oxygen

$$\epsilon_1 \frac{\partial c_{O_2}}{\partial t} = \epsilon_1^{\gamma_1} \frac{\partial}{\partial x}\left(D_{O_2} \frac{\partial c_{O_2}}{\partial x}\right) + \frac{1}{4F} j_2 \quad [6]$$

Modified Ohm's law for the liquid phase

$$\frac{i_2}{\kappa \epsilon_1^{\gamma_1}} = -\frac{\partial \phi_2}{\partial x} - \frac{2RT}{cF}\left(1 - t_-^\circ + \frac{c}{2c_o}\right)\frac{\partial c}{\partial x} \quad [7]$$

Transfer current

$$\frac{\partial i_2}{\partial x} = j_1 + j_2 \quad [8]$$

In the above equations ϵ_1 is the porosity of the positive electrode, γ_1 is the tortuosity factor associated with the porosity, t_-° is the transference number of the anion OH^- with respect to the solvent velocity, D_{OH} is the diffusion coefficient of KOH, D_{O_2} is the apparent diffusion coefficient of oxygen, j_1 and j_2 are the nickel and oxygen transfer currents per unit volume of electrode, and κ is the conductivity of the electrolyte.

The mass transfer of electrolyte (Eq. 5) is considered to be caused only by diffusion and migration; that is, convection has been neglected as suggested by Sinha[18] and Fan and White.[4] The oxygen is treated in the same way as Fan and White[4] did in their model for a nickel/cadmium cell. The mass transfer of oxygen (Eq. 6) is represented using an effective oxygen concentration, c_{O_2}. The effective oxygen concentration accounts for the oxygen in the gas phase and that dissolved in the liquid phase. Equation 7 states that the current density at a given position in the electrolyte inside the electrode results from a gradient in the electrolyte's electric potential and a gradient in electrolyte concentration. The electrochemical reactions that occur in the electrode produce a gradient in the current density in the electrolyte; this is represented by Eq. 8.

During charge and discharge the porosity of the positive electrode, ϵ_1, varies as the active material changes back and forth from NiOOH to $Ni(OH)_2$. However, the variation in porosity is small,[4] and thus the porosity in the nickel electrode is considered to be a constant.

The Butler-Volmer equations is used to express the reaction rates for the nickel and oxygen reactions. The equations are

$$j_1 = a_{Ni} i_{o1,ref}\left\{\left(\frac{c}{c_{ref}}\right)\left(\frac{c_H}{c_{H,ref}}\right)\exp\left[\frac{\alpha_{a1}F}{RT}\eta_1\right] - \left(\frac{c_{H,max} - c_H}{c_{H,max} - c_{H,ref}}\right)\exp\left[-\frac{\alpha_{c1}F}{RT}\eta_1\right]\right\} \quad [9]$$

$$j_2 = a_{Ni} i_{o2,ref}\left\{\left(\frac{c}{c_{ref}}\right)^2\exp\left[\frac{\alpha_{a2}F}{RT}\eta_2\right] - \left(\frac{c_{O_2}}{c_{O_2,ref}}\right)\exp\left[-\frac{\alpha_{c2}F}{RT}\eta_2\right]\right\} \quad [10]$$

in which a_{Ni} is the specific active surface area in the nickel electrode, $i_{o1,ref}$ and $i_{o2,ref}$ are the exchange current densities of the nickel and oxygen reactions evaluated at reference conditions, and c_H is the proton concentration in the active material. The reference concentrations are indicated by the subscript ref. When the active material is completely discharged, the proton concentration takes its maximum value, $c_{H,max}$. The overpotentials in Eq. 9 and 10 are

$$\eta_1 = \phi_1 - \phi_2 - U_{1,ref} \quad [11]$$

$$\eta_2 = \phi_1 - \phi_2 - U_{2,ref} \quad [12]$$

in which ϕ_1 is the potential in the solid phase and $U_{1,ref}$ and $U_{2,ref}$ are the equilibrium potentials at the reference conditions for reactions 1 and 2, respectively. The equilibrium potentials are expressed with respect to an Hg/HgO reference electrode. Assuming that the reference electrode is at the same conditions as the working electrode, the equilibrium potentials for reactions 1 and 2 evaluated at reference conditions are given by

$$U_{1,ref} = U_1^\theta - U_{RE}^\theta - \frac{RT}{F}\ln\left(\frac{c_{H,ref}}{c_{H,max} - c_{H,ref}}\right) \quad [13]$$

$$U_{2,ref} = U_2^\theta - U_{RE}^\theta + \frac{RT}{4F}\ln P_{O_2,ref} \quad [14]$$

where U_1^θ and U_2^θ are the standard potentials for reactions 1 and 2, U_{RE}^θ is the standard potential for the Hg/HgO reaction in alkaline media, and $P_{O_2,ref}$ is the reference oxygen pressure.

In Eq. 9 and 10 we assume that the orders of reaction for NiOOH and OH^- are consistent with the stoichiometry of reactions 1 and 2. The stoichiometry of reaction 2 would predict an order of reaction of 1/2 for O_2 to be used in Eq. 10; however, we assume an order of reaction of 1.0 because there is experimental evidence that the rate of oxygen reduction varies linearly with oxygen pressure.[2] Similar assumptions are made for the kinetics of the reactions taking place in the cadmium electrode, where the oxygen reduction is relevant.

At the center of the positive electrode ($x = 0$) the boundary conditions are

$$\left.\frac{\partial c}{\partial x}\right|_{x=0} = 0 \quad [15]$$

$$\left.\frac{\partial c_{O_2}}{\partial x}\right|_{x=0} = 0 \quad [16]$$

$$\left.\frac{\partial \phi_2}{\partial x}\right|_{x=0} = 0 \quad [17]$$

$$i_2|_{x=0} = 0 \quad [18]$$

Equations 15 and 16 represent the condition of zero flux of electrolyte and oxygen. Equations 17 and 18 indicate that all the current density goes through the solid phase (current collector), thus the potential gradient and the current density in the electrolyte are both equal to zero.

At the interface between the positive electrode and the separator ($x = l_1$) the boundary conditions are

$$\epsilon_1^{\gamma_1}\left.\frac{\partial c}{\partial x}\right|_{x=l_1^-} = \epsilon_2^{\gamma_2}\left.\frac{\partial c}{\partial x}\right|_{x=l_1^+} \quad [19]$$

$$\epsilon_1^{\gamma_1}\left.\frac{\partial c_{O_2}}{\partial x}\right|_{x=l_1^-} = \epsilon_2^{\gamma_2}\left.\frac{\partial c_{O_2}}{\partial x}\right|_{x=l_1^+} \quad [20]$$

$$\epsilon_1^{\gamma_1}\left.\frac{\partial \phi_2}{\partial x}\right|_{x=l_1^-} = \epsilon_2^{\gamma_2}\left.\frac{\partial \phi_2}{\partial x}\right|_{x=l_1^+} \quad [21]$$

$$i_2|_{x=l_1} = i_{cell} \quad [22]$$

in which ϵ_2 is the porosity of the separator, γ_2 is the tortuosity factor associated with the porosity of the separator, and i_{cell} is the applied current density.

Equations 19 and 20 represent the continuity of electrolyte and oxygen flux. Equation 21 represents the continuity of current density in the electrolyte. The current density in the electrolyte is equal to the set current density through the cell, i_{cell} (Eq. 22).

Equations in the y-direction.—The solid particles in the positive electrode are modeled as cylindrical particles that have the substrate along the central axes of the cylinders. The portion filled with substrate has an average radius of y_o. The active material surrounds the substrate, and its thickness is considered to be equal to the average thickness of active material in the original particles, l_y. The proton diffusion in the active material is considered only in the radial direction, y, and is represented by

$$\frac{\partial c_H}{\partial t} = D_H\left(\frac{1}{(y + y_0)}\frac{\partial c_H}{\partial y} + \frac{\partial^2 c_H}{\partial y^2}\right) \quad [23]$$

which is Fick's law in cylindrical coordinates.

Proton diffusion and electron transfer in the active material are assumed to occur simultaneously. Therefore, the current flows only in the radial direction, y, and there is no current flow in the x-direction in the active material. This

results in no generation or consumption of net charge inside the active material. The conservation of charge reduces to the divergence of the current density being equal to zero

$$\frac{\partial \sigma_{Ni}}{\partial y}\frac{\partial \phi_1}{\partial y} + \sigma_{Ni}\left(\frac{\partial^2 \phi_1}{\partial y^2} + \frac{1}{(y + y_0)}\frac{\partial \phi_1}{\partial y}\right) = 0 \quad [24]$$

The conductivity of the active material, σ_{Ni}, is considered a function of the state of charge of the electrode. In the model, we use the correlation found by Antonenko *et al.*,[19] which reads

$$\sigma_{Ni} = 0.1185 \exp(-8.459\theta_P^4) \quad [25]$$

where the state of charge of the nickel electrode, θ_P, is expressed in terms of the proton concentration as

$$\theta_P = \frac{c_H}{c_{H,max}} \quad [26]$$

The boundary conditions at the interface of the electrolyte and the active material ($y = l_y$) are

$$-\sigma_{Ni}\frac{\partial \phi_1}{\partial y}\bigg|_{y=l_y} = \frac{j_1 + j_2}{a_{Ni}} \quad [27]$$

$$-FD_H\frac{\partial c_H}{\partial y}\bigg|_{y=l_y} = \frac{j_1}{a_{Ni}} \quad [28]$$

Equation 27 was obtained assuming that the potential in the active material obeys Ohm's law. Equation 28 indicates that the flux of protons into the active material from the electrolyte is equal to the nickel reaction rate.

The boundary conditions at the interface of the active material and the nickel substrate ($y = 0$) are

$$-D_H\frac{\partial c_H}{\partial y}\bigg|_{y=0} = 0 \quad [29]$$

$$\phi_1|_{y=0} = \phi_{sub} \quad [30]$$

Equation 29 indicates that the flux of protons into the substrate must be zero. At this interface, the potential of the active material must be equal to that of the nickel substrate (Eq. 30).

Separator.—The separator is modeled in one space dimension, x. The governing equations are basically the same as those posed for the positive electrode in the x-direction, but here there are no electrochemical reactions

Material balance on the electrolyte (KOH)

$$\epsilon_2\frac{\partial c}{\partial t} = \epsilon_2^{\gamma_2}\frac{\partial}{\partial x}\left(D_{OH}\frac{\partial c}{\partial x}\right) \quad [31]$$

Material balance on oxygen

$$\epsilon_2\frac{\partial c_{O_2}}{\partial t} = \epsilon_2^{\gamma_2} D_{O_2}\frac{\partial^2 c_{O_2}}{\partial x^2} \quad [32]$$

Modified Ohm's law for the liquid phase

$$\frac{i_2}{\kappa\epsilon_2^{\gamma_2}} = -\frac{\partial \phi_2}{\partial x} - \frac{2RT}{cF}\left(1 - t_-^\circ + \frac{c}{2c_o}\right)\frac{\partial c}{\partial x} \quad [33]$$

Potential in the solid phase

$$\phi_1 = 0 \quad [34]$$

Current in the electrolyte

$$i_2 = i_{cell} \quad [35]$$

Equations 31 and 32 represent the mass transfer of electrolyte and oxygen in the absence of electrochemical reactions. The current density in the liquid phase is equal to the cell's current density (Eq. 35), because the solid material in the separator is an electrical insulator (Eq. 34). As in the positive electrode, the current density, the potential, and the concentration of electrolyte in the liquid phase are related by Ohm's law (Eq. 33).

Negative electrode.—The negative electrode is modeled in one spatial dimension, x. The governing equations are the same as those posed for the positive electrode in the x-direction. In addition to these equations, the conservation of charge and the variation in porosity are introduced. The equations for this electrode are those presented by Fan and White[4]

Material balance of electrolyte (KOH)

$$\frac{\partial(\epsilon_3 c)}{\partial t} = \frac{\partial}{\partial x}\left(\epsilon_3^{\gamma_3} D_{OH}\frac{\partial c}{\partial x}\right) + \frac{(t_-^\circ - 1)}{F}\frac{\partial i_2}{\partial x} \quad [36]$$

Material balance of oxygen

$$\frac{\partial(\epsilon_3 c_{O_2})}{\partial t} = \frac{\partial}{\partial x}\left(\epsilon_3^{\gamma_3} D_{O_2}\frac{\partial c_{O_2}}{\partial x}\right) + \frac{1}{4F} j_4 \quad [37]$$

Modified Ohm's law for the liquid phase

$$\frac{i_2}{\kappa\epsilon_3^{\gamma_3}} = -\frac{\partial \phi_2}{\partial x} - \frac{2RT}{cF}\left(1 - t_-^\circ + \frac{c}{2c_o}\right)\frac{\partial c}{\partial x} \quad [38]$$

Conservation of charge

$$i_2 - \sigma_{Cd}\theta_N^\beta\frac{\partial \phi_1}{\partial x} = i_{cell} \quad [39]$$

Transfer current

$$\frac{\partial i_2}{\partial x} = j_3 + j_4 \quad [40]$$

Porosity variation

$$\frac{\partial \epsilon_3}{\partial t} = \frac{1}{2F}\left(\frac{M_{Cd}}{\rho_{Cd}} - \frac{M_{Cd(OH)_2}}{\rho_{Cd(OH)_2}}\right) j_3 \quad [41]$$

In these equations ϵ_3 is the porosity of the negative electrode, γ_3 is the tortuosity factor associated to the porosity of the electrode, σ_{Cd} is the conductivity of the solid material in the electrode, θ_N is the state of charge of the negative electrode (see below), β is the tortuosity factor associated to the porosity of the solid material in the cadmium electrode, j_3 and j_4 are the cadmium and oxygen reaction currents per unit of volume, M_i is the molecular weight of species i, and ρ_i is the density of species i.

The conservation of charge is represented by Ohm's law in the solid phase (Eq. 39). The porosity of the negative electrode varies as the solid material changes from Cd to $Cd(OH)_2$. Therefore, the rate at which the porosity changes is considered to be proportional to the rate of the cadmium reaction (Eq. 41).

The kinetic expressions for the cadmium and oxygen reactions are

$$j_3 = a_{Cd}\theta_N^\beta i_{o3,ref}\left\{\left(\frac{c}{c_{ref}}\right)^2 \exp\left[\frac{\alpha_{a3}F}{RT}\eta_3\right] - \exp\left[-\frac{\alpha_{c3}F}{RT}\eta_3\right]\right\} \quad [42]$$

$$j_3 = a_{Cd}\theta_N^\gamma i_{o4,ref}\left\{\left(\frac{c}{c_{ref}}\right)^2 \exp\left[\frac{\alpha_{a4}F}{RT}\eta_4\right] - \left(\frac{c_{O_2}}{c_{O_2,ref}}\right)\exp\left[-\frac{\alpha_{c4}F}{RT}\eta_4\right]\right\} \quad [43]$$

The local state of charge of the negative electrode, θ_N, can be expressed as a function of electrode porosity

$$\theta_N = \frac{\epsilon_3 - \epsilon_{3,min}}{\epsilon_{3,max} - \epsilon_{3,min}} \quad [44]$$

The porosity of the electrode takes its maximum value, $\epsilon_{3,max}$, when the electrode is fully charged. When the electrode is completely discharged the porosity takes its minimum value, $\epsilon_{3,min}$.

The overpotentials in Eq. 42 and 43 are

$$\eta_3 = \phi_1 - \phi_2 - U_{3,ref} \quad [45]$$

$$\eta_4 = \phi_1 - \phi_2 - U_{4,ref} \quad [46]$$

in which $U_{3,ref}$ and $U_{4,ref}$ are the equilibrium potentials at reference conditions for reactions 3 and 4, respectively. The equilibrium potentials are expressed with respect to an Hg/

HgO reference electrode in the same way as we did for reactions 1 and 2 in the nickel electrode. The equilibrium potentials for reactions 3 and 4 evaluated at reference conditions are given by

$$U_{3,\text{ref}} = U_3^\theta - U_{\text{RE}}^\theta \quad [47]$$

$$U_{4,\text{ref}} = U_4^\theta - U_{\text{RE}}^\theta + \frac{RT}{4F} \ln P_{O_2,\text{ref}} \quad [48]$$

where U_3^θ and U_4^θ are the standard potentials for reactions 3 and 4, respectively. In Eq. 47 we have assumed that the activity of the solid species Cd and $Cd(OH)_2$ is unity at the reference conditions. In Eq. 42 and 43 we have assumed that the orders of reaction for OH^- are consistent with the stoichiometry of reactions 3 and 4. As mentioned before for the positive electrode, the order of reaction for oxygen used in Eq. 43 is assumed to be 1.0 because the rate of oxygen reduction varies linearly with oxygen pressure.[2]

The boundary conditions at the interface between the negative electrode and the separator ($x = l_1 + l_2$) are

$$\epsilon_2^{\gamma_2} \left.\frac{\partial c}{\partial x}\right|_{x=l_1+l_2^-} = \epsilon_3^{\gamma_3} \left.\frac{\partial c}{\partial x}\right|_{x=l_1+l_2^+} \quad [49]$$

$$\epsilon_2^{\gamma_2} \left.\frac{\partial c_{O_2}}{\partial x}\right|_{x=l_1+l_2^-} = \epsilon_3^{\gamma_3} \left.\frac{\partial c_{O_2}}{\partial x}\right|_{x=l_1+l_2^+} \quad [50]$$

$$\left.\frac{\partial \phi_1}{\partial x}\right|_{x=l_1+l_2} = 0 \quad [51]$$

$$\epsilon_2^{\gamma_2} \left.\frac{\partial \phi_2}{\partial x}\right|_{x=l_1+l_2^-} = \epsilon_3^{\gamma_3} \left.\frac{\partial \phi_2}{\partial x}\right|_{x=l_1+l_2^+} \quad [52]$$

$$i_2|_{x=l_1+l_2} = i_{\text{cell}} \quad [53]$$

$$\frac{\partial \epsilon_3}{\partial t} = \frac{1}{2F}\left(\frac{M_{Cd}}{\rho_{Cd}} - \frac{M_{Cd(OH)_2}}{\rho_{Cd(OH)_2}}\right) j_{Cd} \quad [54]$$

The boundary conditions at the center of the negative electrode current collector ($x = l$) are

$$\left.\frac{\partial c}{\partial x}\right|_{x=l} = 0 \quad [55]$$

$$\left.\frac{\partial c_{O_2}}{\partial x}\right|_{x=l} = 0 \quad [56]$$

$$\left.\frac{\partial i_2}{\partial x}\right|_{x=l} = j_{Cd} + j_{O_2} \quad [57]$$

$$\left.\frac{\partial \phi_2}{\partial x}\right|_{x=l} = 0 \quad [58]$$

$$i_2|_{x=l} = 0 \quad [59]$$

$$\frac{\partial \epsilon_3}{\partial t} = \frac{1}{2F}\left(\frac{M_{Cd}}{\rho_{Cd}} - \frac{M_{Cd(OH)_2}}{\rho_{Cd(OH)_2}}\right) j_{Cd} \quad [60]$$

Except for the condition on the electrode porosity, the boundary conditions at both ends of the negative electrode are the same as those in the positive electrode.

The equations for the model, as described above, were solved using finite differences with an implicit stepping technique for the time derivatives. The value for the parameters involved in the equations are listed in Table I. The relations presented in Eq. 61-67 were used to estimate some physical parameters of the nickel and cadmium electrode presented in Table I. Equations 62 through 65 were presented by Mao *et al.*[15] and were derived assuming that the porosity for the nickel substrate, $\epsilon_{o,P}$, and the theoretical charge, Q_{max}, are known, and that the nickel substrate consists of a collection of cylinders covered with a layer of active material (see Fig. 1)

Maximum proton concentration

$$c_{H,\max} = \frac{\rho_{Ni(OH)_2}}{M_{Ni(OH)_2}} \quad [61]$$

Porosity of the nickel electrode

$$\epsilon_1 = \epsilon_{o,P} - \frac{Q_{\max}}{F c_{H,\max} l_1} \quad [62]$$

Radius of the nickel substrate in cylindrical shape

$$y_o = \frac{2(1-\epsilon_{o,P})}{a_o} \quad [63]$$

Thickness of the active material

$$l_y = y_o \sqrt{1 + \frac{2(\epsilon_{o,P} - \epsilon_1)}{y_o a_o}} - y_o \quad [64]$$

Specific active surface area of the nickel electrode

$$a_{Ni} = a_o \sqrt{\frac{1-\epsilon_1}{1-\epsilon_{o,P}}} \quad [65]$$

Minimum porosity of the cadmium electrode

Table I. Value of the model parameters used in the simulations.

Parameter	Value	Source
a_{Cd}	4000 $cm^2\ cm^{-3}$	
a_{Ni}	3864 $cm^2\ cm^{-3}$	Eq. 65
a_o	2000 $cm^2\ cm^{-3}$	
c_{ref}	7.1×10^{-3} mol cm^{-3}	
$c_{H,max}$	5.209×10^{-2} mol cm^{-3}	Eq. 61
$c_{H,ref}$	0.5 $c_{H,max}$	
$c_{O_2,ref}$	10^{-7} mol cm^{-3} [a]	Ref. 25
D_H	4.6×10^{-11} $cm^2\ s^{-1}$	Ref. 8
D_{O_2}	10^{-3} $cm^2\ s^{-1}$	
F	96,487 C mol^{-1}	
$i_{o1,ref}$	6.1×10^{-5} A cm^{-2}	Ref. 18
$i_{o2,ref}$	1.0×10^{-11} A cm^{-2}	Ref. 2
$i_{o3,ref}$	6.1×10^{-5} A cm^{-2}	
$i_{o4,ref}$	1.0×10^{-14} A cm^{-2}	
l	0.101 cm ($l_1 + l_2 + l_3$)	
l_1	0.036 cm	Ref. 1
l_2	0.025 cm	Ref. 1
l_3	0.040 cm	Ref. 1
l_y	1.4×10^{-4} cm	Eq. 64
L_{neg}	2.3 g of $Cd(OH)_2$	Ref. 1
M_{Cd}	112.4 g mol^{-1}	
$M_{Cd(OH)_2}$	146.4 g mol^{-1}	
$M_{Ni(OH)_2}$	92.71 g mol^{-1}	
$P_{O_2,ref}$	1 atm	
Q_{max}	74.16 C cm^{-2} of electrode (20.6×10^{-3} Ah cm^{-2} of electrode)[b]	Ref. 1
R	8.3143 J mol^{-1} K^{-1}	
T	298.15 K	
U_{RE}^θ	0.0983 V	Ref. 22
$U_1^\theta - U_{RE}^\theta$	0.427 V	Ref. 20
U_2^θ	0.401 V	Ref. 22
U_3^θ	−0.808 V	Ref. 22
U_4^θ	0.401 V	Ref. 22
$U_{1,ref}$	0.427 V *vs.* Hg/HgO	Eq. 13
$U_{2,ref}$	0.3027 V *vs.* Hg/HgO	Eq. 14
$U_{3,ref}$	−0.9063 V *vs.* Hg/HgO	Eq. 47 (Ref. 22)
$U_{4,ref}$	0.3027 V *vs.* Hg/HgO	Eq. 48 (Ref. 22)
y_o	1.5×10^{-4} cm	Eq. 63
α_{a1}	0.5	
$\alpha_{c1} = 1 - \alpha_{a1}$	0.5	
α_{a2}	1.5	
$\alpha_{c2} = 2 - \alpha_{a2}$	0.5	
α_{a3}	1.0	
$\alpha_{c3} = 2 - \alpha_{a3}$	1.0	
α_{a4}	1.5	
$\alpha_{c4} = 1 - \alpha_{a4}$	0.5	
β	0:5	
$\epsilon_{o,P}$	0.85	Ref. 1
$\epsilon_{o,N}$	0.80	Ref. 1
ϵ_1	0.44	Eq. 62
ϵ_2	0.68	Ref. 1
$\epsilon_{3,max}$	0.64	Eq. 67
$\epsilon_{3,min}$	0.42	Eq. 66
ϕ_{sub}	0.427 V (arbitrary value)	
γ_1	1.5	
γ_2	1.5	
γ_3	1.5	
ρ_{Cd}	8.64 g cm^{-3}	Ref. 1
$\rho_{Cd(OH)_2}$	4.79 g cm^{-3}	Ref. 1
$\rho_{Ni(OH)_2}$	4.83 g cm^{-3}	Ref. 1
σ_{Cd}	1.4706×10^5 S cm^{-1} [c]	Ref. 23
τ	1	

[a] Solubility of oxygen in a 35% weight KOH electrolytic solution in equilibrium with an oxygen atmosphere at 1 atm.
[b] Corresponds to a loading of approximately 2.0 g of $Ni(OH)_2/cm^3$ void.
[c] Conductivity of pure cadmium.

Table II. Properties of the electrolyte (KOH aqueous solution).

Diffusion coefficient, D_{OH}
Using experimental data reported for the integral diffusion coefficient at 25°C for electrolyte concentrations in the range 0.103 to 13.719×10^{-3} mol cm^{-3},[21] we obtained

$$\overline{D}_{OH} = \exp(-10.467 - 8.1607\, c^{1/2} + 286.2\, c - 2539.8\, c^{3/2} + 7207.5\, c^2)$$

The regression had an average relative error of 0.36%. The differential diffusion coefficient,[16,21] which is the one we need in Eq. 5, 31, and 36, is given by

$$D_{OH} = \overline{D}_{OH}\left(c\frac{d\overline{D}_{OH}}{dc} + 1\right) = \overline{D}_{OH}(1.0 - 4.0804\, c^{1/2} + 286.2\, c - 3809.7\, c^{3/2} + 14415.0\, c^2)$$

Specific conductivity, κ
The following expression was obtained for the specific conductivity of the free-electrolyte using experimental data for the equivalent conductance at 25°C for electrolyte concentrations in the range 0.06081 to 10.611×10^{-3} mol cm^{-3}[21]

$$\kappa = c \exp(5.5657 - 6.1538\, c^{1/2} + 13.408\, c - 1075.8\, c^{3/2})$$

The regression had an average relative error of 0.16%.

Ratio of electrolyte concentration to water concentration, c/c_o
Using experimental data for the density of the electrolyte at 25°C,[21] we obtained the following expression for c/c_o

$$\frac{c}{c_o} = \exp(-6.8818 + 118.75\, c^{1/2} - 1030.5\, c + 4004.7\, c^{3/2})$$

The experimental data used for the regression is for electrolyte concentrations in the range 0.3617 to 13.449×10^{-3} mol cm^{-3}. The regression had an average relative error of 1.67%.

The transference number, t_-° is constant and equal to 0.78 for electrolyte concentrations in the range 2.89 to 10.04×10^{-3} mol cm^{-3}.[2]

$$\epsilon_{3,min} = \epsilon_{o,N}\left(1 - \frac{L_{neg}}{\rho_{Cd(OH)_2}}\right) \quad [66]$$

Maximum porosity of the cadmium electrode

$$\epsilon_{3,max} = \epsilon_{o,N}\left(1 - \frac{L_{neg}}{\rho_{Cd}}\frac{M_{Cd}}{M_{Cd(OH)_2}}\right) \quad [67]$$

The properties D_{OH}, κ, and c/c_o are functions of the electrolyte concentration, c. We obtained correlations for these properties by fitting polynomials on $c^{1/2}$ to the logarithm of each property. The resulting correlations are presented in Table II. The initial conditions used for charge and discharge simulations are listed in Table III.

Sensitivity Analysis

We performed a sensitivity analysis to determine the effect of the various parameters included in the model on the simulated cell behavior. The processes associated with those parameters with the largest sensitivities are the most influential in predicting cell behavior. We have used this method to evaluate the impact of including the proton diffusion and ohmic drop in the active material of the nickel electrode in a model for an Ni-Cd cell.

First, we need to define what we call the behavior of a cell. The model can be used to simulate several responses of an Ni-Cd cell, such as, concentration, potential, and current profiles inside the cell. We choose two responses of the cell that can be simulated with the model and that are of practical interest. the predicted cell voltage as a function of time and the amount of charge present in the nickel electrode at the end of an operation (charge and discharge efficiency). We calculated sensitivity coefficients for the parameters involved in the appropriate equations. The larger the sensitivity coefficient of one parameter with respect to those of the other parameters, the larger is the effect of that parameter on the response being considered. The processes being considered and their associated parameters are listed in Table IV.

The sensitivity coefficient of parameter p on the cell voltage, V_{cell}, is S_p^V and is defined as

$$S_p^V = \frac{\partial V_{cell}}{\partial p/p} \quad (V) \quad [68]$$

For each of the parameters included in Table IV, the coefficient S_p^V is computed over time during charge and discharge operations.

The sensitivity coefficient of parameter p over the amount of charge (amount of NiOOH) present in the nickel electrode at the end of a discharge or charge operation is defined as

$$S_p^Q = \frac{\partial Q/Q_{max}}{\partial p/p} \quad [69]$$

in which Q is the amount of charge in the nickel electrode and is calculated as

$$Q = \frac{(1-\epsilon_1)F}{\pi(y_o + l_y)^2}\int_{x=0}^{x=l_1}\int_{y=0}^{y=l_y} 2\pi(y + y_o)(c_{H,max} - c_H)dydx\left(\frac{C}{\text{cm}^2 \text{ of electrode}}\right) \quad [70]$$

The coefficient S_p^Q is computed at the cutoff voltage of 0.9 V for the discharge operation and at a given time during overcharge. To compute the sensitivity coefficients, we use the following approximations

$$S_p^V \approx \frac{\Delta V_{cell}}{\Delta p/p} \quad [71]$$

$$S_p^Q \approx \frac{\Delta Q/Q_{max}}{\Delta p/p} \quad [72]$$

in which Δp is a small change in the parameter p with respect to its base value, and ΔV_{cell} and ΔQ are the resulting changes in V_{cell} and Q, respectively. The base value of all the parameters is shown in Table I. The change in the parameter was chosen such that a forward ($\Delta p > 0$) and backward difference ($\Delta p < 0$) from the base value gave the same computed sensitivity coefficient. In most cases, the commonly used 1% change on the base value of the parameter[24] was appropriate.

Results and Discussion

Several of the plots presented here are given as a function of the state-of-discharge and state-of-charge of the Ni-Cd cell, which we define as follows

State-of-discharge during a discharge operation

$$SOD = \frac{-i_{cell}t}{Q_{max}} \text{ with } i_{cell} < 0 \quad [73]$$

State-of-charge during a charge operation

$$SOC = \frac{i_{cell}t}{Q_{max}} \text{ with } i_{cell} > 0 \quad [74]$$

The states of discharge and charge are defined as that of the nickel electrode because the Ni-Cd cell is positive limited. The predicted cell voltage is defined as follows

$$V_{cell} = \phi_1(x = 0, y = 0) - \phi_1(x = l) \quad [75]$$

Table III. Initial conditions used in the simulations.

Variable	Positive electrode charge/discharge	Separator charge/discharge	Negative electrode charge/discharge
c	7.1×10^{-3}/ 7.1×10^{-3} mol cm^{-3}	7.1×10^{-3}/ 7.1×10^{-3} mol cm^{-3}	7.1×10^{-3}/ 7.1×10^{-3} mol cm^{-3}
c_{O_2}	$10^{-20}/10^{-20}$ mol cm^{-3}	$10^{-20}/10^{-20}$ mol cm^{-3}	$10^{-20}/10^{-20}$ mol cm^{-3}
i_2	0/0	0/0	0/0
ϕ_2	solve Eq. 9 for $j_1 = 0$/ solve Eq. 9 for $j_1 = 0$	same ϕ_2 as in positive/ same ϕ_2 as in positive	same ϕ_2 as in positive/ same ϕ_2 as in positive
ϕ_1	ϕ_{sub}/ϕ_{sub}	0/0	solve Eq. 42 for $j_3 = 0$/ solve Eq. 42 for $j_3 = 0$
c_H	5.1569×10^{-3}/ 1.0418×10^{-3} mol cm^{-3}	—	—
ϵ	—	—	0.47/0.64

In Eq. 75, the first term is the potential in the nickel substrate at the center of the nickel electrode and the second term is the potential in the solid phase at the center of the cadmium electrode.

Discharge characteristics.—Figure 2 presents curves for the predicted cell voltage during discharge for three discharge rates. The curves are consistent with the real behavior of a cell during discharge in regard to the decrease of the discharge potential as the discharge rate is increased. Figure 3 shows the same discharge curves as a function of the SOD of the cell. These curves show the characteristic decrease in the SOD at the end of the discharge operation (cutoff voltage of 0.9 V) as the discharge rate is increased. This behavior is caused by a slow proton diffusion process relative to the electrochemical reaction (Eq. 1) that takes place on the surface of the active material in the nickel electrode. During discharge, the proton concentration at the surface of the active material ($y = l_y$) increases because of the main electrochemical reaction (Eq. 1). As the proton concentration increases, the overpotential of the nickel electrode increases causing the cell potential to decrease, and when it reaches the maximum proton concentration, $c_{H,max}$, the cell potential drops sharply. The accumulation of protons at the surface of the active material depends on the relative rate between the electrochemical reaction and the proton diffusion into the bulk of the active material. As the discharge rate is increased, the electrochemical reaction rate (j_1) increases, the proton concentration at the surface of the active material reaches $c_{H,max}$ sooner, and a sharp drop in the potential of the cell occurs earlier. Thus, increasingly more active material is left unreacted in the nickel electrode as the discharge rate is increased.

Figure 4 shows the sensitivity coefficient of various parameters on the predicted cell voltage as defined by Eq. 71. The sensitivity coefficients are given as a function of the SOD for a discharge operation at $C/2.1$ rate (-10 mA cm^{-2}). In this plot we show only the results for the parameters that have the largest sensitivities. At the beginning of discharge the largest sensitivity is that of the exchange current density of the main reaction in the nickel electrode, $i_{o1,ref}$. As the discharge proceeds, the sensitivity coefficient of the transfer coefficient α_{a1} increases until it becomes the largest. Therefore, the kinetic parameters of the main reaction of the nickel electrode (Eq. 1) has the largest effect on the discharge voltage during almost the entire operation. However, toward the end of discharge ($SOD \approx 0.95$) the sensitivity of the proton diffusion coefficient becomes important also, and the predicted cell voltage is affected by both the kinetics of the nickel reaction and proton diffusion into the active material. If the cell is discharged at a higher rate ($C/0.7$), the sensitivity coefficients for the various parameters exhibit a similar behavior as those for a $C/2.1$ rate. In Fig. 5 we can see the results for the largest sensitivity coefficients for both rates, and these are those for $i_{o1,ref}$, α_{a1}, and D_H. As the rate of discharge is increased, the sensitivity coefficients become larger, but the most important parameters are the same for both rates. However, the sharp increase in the sensitivity coefficient for the proton diffusion coefficient takes place at a smaller SOD for the $C/0.7$ rate ($SOD \approx 0.9$). This means that the portion of the discharge operation during which the proton diffusion affects the cell voltage widens as the rate of discharge is increased.

In addition to the predicted cell voltage during discharge, we considered the amount of charge left in the nickel electrode at the end of discharge as a response of interest, because it reflects the discharge efficiency. The sensitivity coefficient of a parameter on this response is given by Eq. 72. Figure 6 shows the results for the largest sensitivity coefficients for discharge rates of $C/2.1$ and $C/0.7$. The most important parameter is the proton diffusion coefficient D_H, followed by the anodic transfer coefficient of the nickel reaction, α_{a1}. This means that the discharge efficiency is mostly affected by the proton diffusion process and the kinetics of the nickel reaction with the proton diffusion having the largest effect. Both processes affect the discharge efficiency of the cell, and their relative importance varies with operating conditions. For example, in Fig. 6 we can see that the sensitivity of D_H for a discharge rate of $C/0.7$ is approximately 2.5 times that for a $C/2.1$ rate; however, the sensitivity of α_{a1} for $C/0.7$ is approximately five times that for $C/2.1$ rate. Thus, the relative effect of D_H and α_{a1} on the discharge efficiency changes with

Table IV. Model parameters used in the sensitivity analysis.

Process	Parameter
Nickel reaction in the positive electrode	$i_{o1,ref}$ and α_{a1}
Oxygen reaction in the positive electrode	$i_{o2,ref}$ and α_{a2}
Cadmium reaction in the negative electrode	$i_{o3,ref}$ and α_{a3}
Oxygen reaction in the negative electrode	$i_{o4,ref}$ and α_{a4}
Proton diffusion	D_H
Ohmic drop in the active material in the nickel electrode	σ_{Ni}
Ohmic drop in the electrolyte	κ and t_-^o
Mass transfer of electrolyte	D_{OH} and t_-^o
Mass transfer of oxygen	D_{O_2}

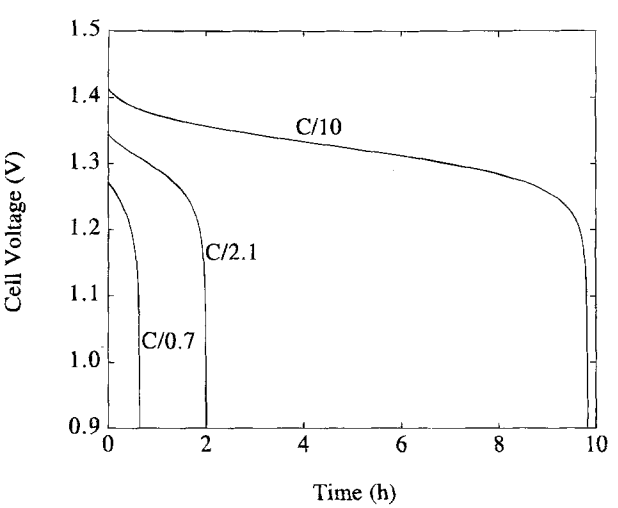

Fig. 2. Predicted cell voltage as a function of time during a discharge operation for three discharge rates (C rate = 20.6 mA cm^{-2}).

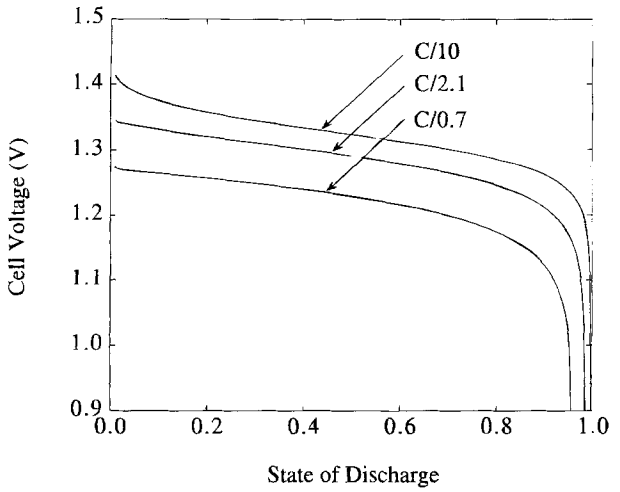

Fig. 3. Predicted cell voltage as a function of the SOD during a discharge operation for three discharge rates. The SOD is defined in Eq. 73.

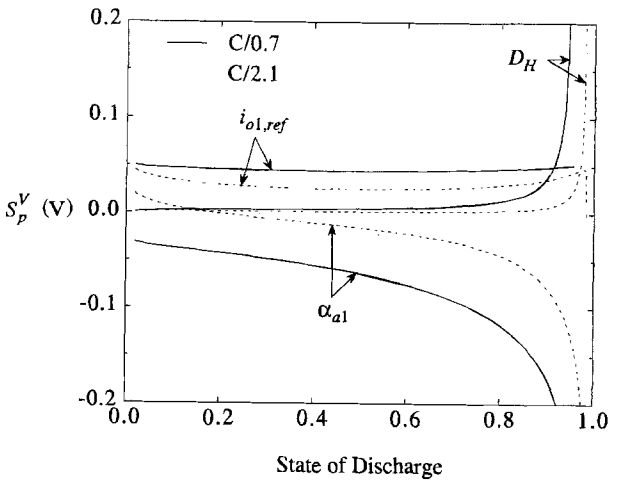

Fig. 5. Largest computed sensitivity coefficients on the predicted cell voltage during discharge for two discharge rates: (- - -) C/2.1 and (—) C/0.7.

the discharge rate, and the effect of D_H is larger at the higher discharge rate. The sign of the sensitivity coefficients indicates that the amount of charge left in the nickel electrode at the end of discharge decreases as D_H increases and it increases as α_{a1} increases. There is more charge drained from the cell if the proton diffusion process is faster relative to the rest of the processes, especially relative to the rate of the nickel reaction.

In summary, the kinetic parameters of the main reactions in both electrodes and the proton diffusion coefficient are the most important parameters affecting the predicted cell voltage and efficiency during discharge. The kinetics of the main reaction in the nickel electrode is the leading factor in predicting the cell voltage during discharge, with the proton diffusion having a smaller effect limited to the very last portion of the discharge process. However, the proton diffusion is the main factor influencing the predictions for discharge efficiency, that is, the total charge drained from the cell during discharge.

Charge characteristics.—Simulations of the charge operation are readily obtained using the same model and changing the sign of the applied current density. Figure 7 shows predicted charge curves for three different rates. The curves exhibit the characteristic overcharge plateau toward the end of the charge process due to the oxygen evolution at the nickel electrode and reduction at the cadmium electrode. As the charge rate increases, the cell potential rises more sharply, and the overcharge voltage increases. Also, the roll-over of the voltage curve at the beginning of overcharge becomes apparent as the charge rate increases. This is caused by the large overpotentials of the oxygen evolution at the nickel electrode and that of the oxygen reduction at the cadmium electrode right after reactions 2 and 4 begin. As the electrochemical reduction of oxygen proceeds in the cadmium electrode, the oxygen concentration decreases, and the overpotential decreases (see Eq. 43); thus, the cell voltage is reduced.

We computed the sensitivity coefficients for the same parameters and responses as for the discharge operation. Figure 8 shows the results for the parameters that have the largest sensitivity coefficients on the cell voltage during charge at C/2.1 rate. Before the oxygen evolution reaction begins ($SOC \approx 0.9$), the voltage of the cell is mostly affected by the kinetics of the nickel and cadmium reactions, as shown in Fig. 8. When the oxygen evolution reaction begins ($SOC > 0.9$) the sensitivity of the transfer coefficient for oxygen evolution (α_{a2}) increases rapidly as the other sensitivity coefficients tend to zero. Thus, the predicted cell voltage during overcharge is affected almost exclusively by the oxygen reaction. For a larger rate of charge of C/0.7, the largest sensitivity coefficients correspond to the same set of parameters as for C/2.1, as shown in Fig. 9.

Figure 10 shows the largest sensitivity coefficients of the parameters on the amount of charge at the end of charge. The end of charge was considered to be at $t = 2.52$ h for a

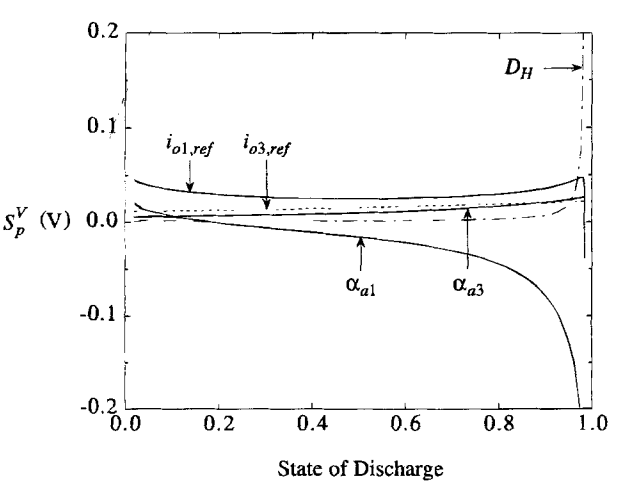

Fig. 4. Largest computed sensitivity coefficients on the predicted cell voltage during discharge at C/2.1 rate.

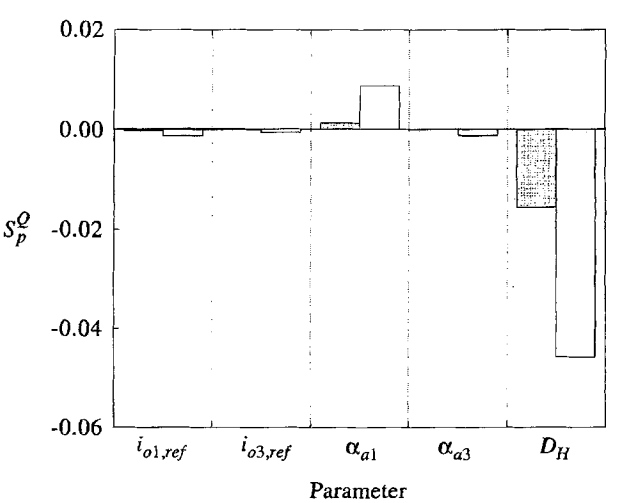

Fig. 6. Largest computed sensitivity coefficients on the amount of charge left in the nickel electrode at the end of discharge (0.9 V) for two discharge rates. The gray columns are for C/2.1 rate and the white columns are for C/0.7.

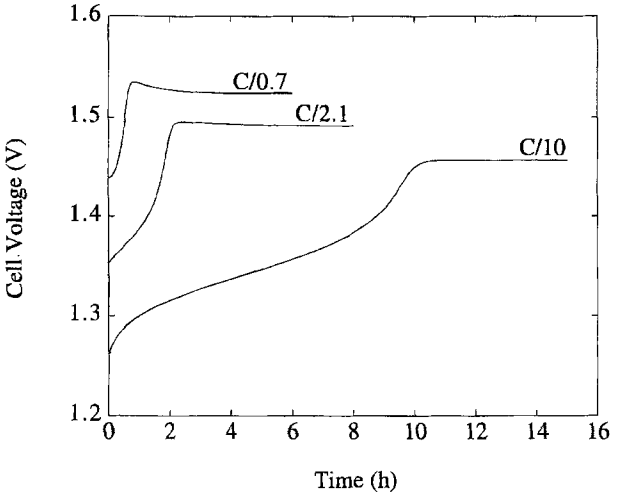

Fig. 7. Predicted voltage of the cell as a function of time during a charge operation for three charge rates.

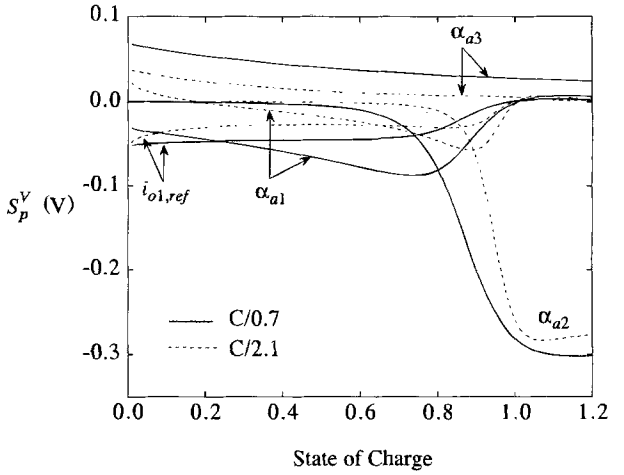

Fig. 9. Largest computed sensitivity coefficients on the predicted cell voltage during charge for two charge rates: (- - -) C/2.1 and (—) C/0.7. The SOC is defined in Eq. 74.

charge rate of $C/2.1$ and at $t = 0.84$ h for $C/0.7$; that is, an overcharge of 20% over the theoretical time that it would take to charge the nickel electrode fully. The results shown in Fig. 10 indicate that the transfer coefficient for the oxygen evolution, α_{a2}, has the largest effect on the amount of charge present in the nickel electrode by the end of charge. The next most important parameter is the transfer coefficient of the nickel reaction, α_{a1}. Also, the sign of the sensitivity coefficients indicates that the amount of charge decreases if α_{a2} is increased and it increases if α_{a1} is increased. The larger the rate of oxygen evolution the larger is the amount of current used in this reaction, and thus, the current used in the main nickel reaction is smaller leading to less charge in the electrode.

Conclusion

The incorporation of proton diffusion in the nickel electrode in the model for an Ni-Cd cell improves the simulation capabilities of the model, particularly for the discharge process. For the operating conditions considered in this work, the magnitude of the ohmic drop in the active material is small compared to the overall potential drop in the nickel electrode and was shown to have a negligible effect on cell behavior during charge and discharge operations. The most important factors affecting the discharge behavior are the kinetics of the nickel reaction and the proton diffusion process. The discharge efficiency (utilization of active material) is mostly affected by proton diffusion. For the charge operation, the kinetics of the nickel and cadmium reactions affect the predicted cell voltage almost equally. These two reactions are the most important factors in determining the cell voltage during charge before oxygen evolution begins at the nickel electrode; at which time the kinetics of the oxygen evolution become the only relevant process affecting the cell voltage. Likewise, the amount of charge that is input into the cell at the end of a charge operation (charge efficiency) is mostly affected by the oxygen evolution kinetics. The effect of mass transfer and ohmic drop in the electrolyte during charge and discharge is considerably smaller than those just mentioned. In view of these results, one may consider the option of neglecting the mass transfer and ohmic drop in the electrolyte for an approximate and simpler mathematical model of an Ni-Cd cell. However, if one is interested in predicting the electrolyte concentration and potential distribution inside the cell, these processes must be included in a model of an Ni-Cd cell. From the results presented here, it appears evident that any modeling effort for an Ni-Cd cell benefits largely from any improvement in the representation of the electrode processes: main electrochemical reactions, oxygen evolution reaction, and proton diffusion.

The model presented here can be used to estimate the parameters that were shown to have the largest sensitivi-

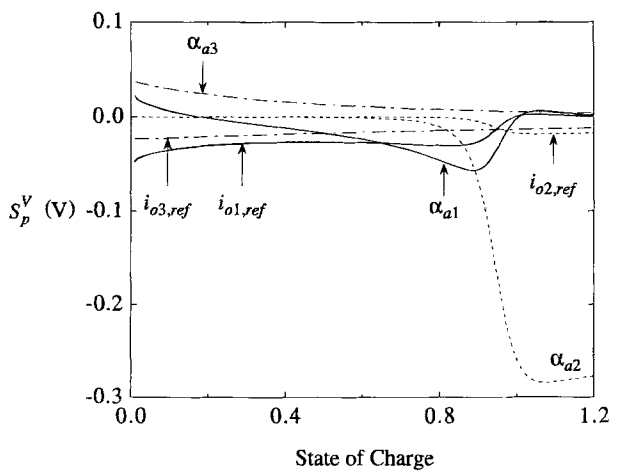

Fig. 8. Largest computed sensitivity coefficients on the predicted cell voltage during charge at C/2.1 rate. The SOC is defined in Eq. 74.

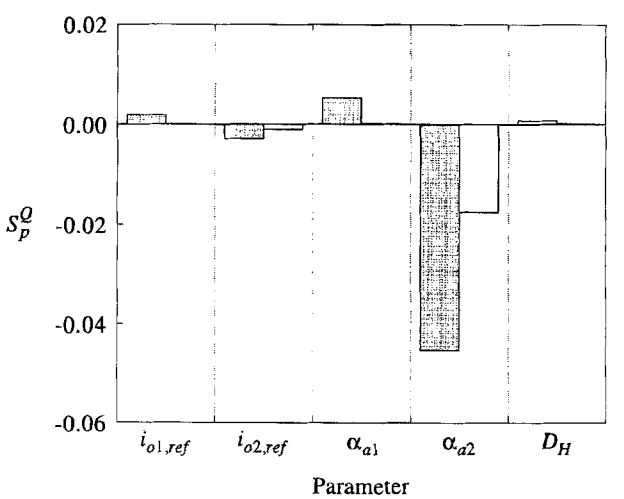

Fig. 10. Largest computed sensitivity coefficients on the amount of charge present in the nickel electrode at the end of charge operation for two charge rates. The end of charge is taken at $t = 2.52$ h for a rate of C/2.1 and at $t = 0.84$ h for C/0.7 (equivalent to 20% of overcharge). The gray columns are for C/2.1 rate and the white columns are for C/0.7.

ties on the cell behavior. The experimental data must be collected for conditions under which the parameters have their largest sensitivities. Also, this model can be used to predict battery performance during charge and discharge operations. Therefore, it can assist battery designers and engineers in studying the effect of various design parameters on battery performance.

Acknowledgment

The authors are grateful for the financial support for this work from the Jet Propulsion Laboratory, the NASA Center for Space Power at Texas A&M University, and the Office of Research and Development of the United States Central Intelligence Agency.

Manuscript submitted Sept. 27, 1994; revised manuscript received Dec. 22, 1994.

University of South Carolina assisted in meeting the publication costs of this article.

LIST OF SYMBOLS

a_{Cd} specific active surface area in the cadmium (negative) electrode, $cm^2\ cm^{-3}$
a_{Ni} specific active surface area in the nickel (positive) electrode, $cm^2\ cm^{-3}$
a_o specific surface area of the nickel substrate in the positive electrode, $cm^2\ cm^{-3}$
c concentration of the electrolyte, KOH, mol cm^{-3}
c_o concentration of water, mol cm^{-3}
c_{ref} reference concentration of the binary electrolyte, KOH, mol cm^{-3}
c_H proton concentration in the active material, mol cm^{-3}
$c_{H,max}$ proton concentration in the active material at fully discharge state, mol cm^{-3}
$c_{H,ref}$ reference proton concentration in the active material, mol cm^{-3}
c_{O_2} effective oxygen concentration, mol cm^{-3}
$c_{O_2,ref}$ effective reference oxygen concentration, mol cm^{-3}
D_H diffusion coefficient of protons, $cm^2\ s^{-1}$
D_{OH} diffusion coefficient of KOH, $cm^2\ s^{-1}$
D_{O_2} apparent diffusion coefficient of oxygen, $cm^2\ s^{-1}$
F Faraday's constant, 96,487 C mol^{-1}
i_2 current density in the liquid phase based on the projected electrode area, A cm^{-2}
i_{cell} applied current density, A cm^{-2}
$i_{o1,ref}$ exchange current density of the nickel reaction at reference conditions, A cm^{-2} of active surface area
$i_{o2,ref}$ exchange current density of the oxygen reaction in the nickel electrode at reference conditions, A cm^{-2} of active surface area
$i_{o3,ref}$ exchange current density of the cadmium reaction at reference conditions, A cm^{-2} of active surface area
$i_{o4,ref}$ exchange current density of the oxygen reaction in the cadmium electrode at reference conditions, A cm^{-2} of active surface area
j_1 nickel reaction current per unit volume of positive electrode, A cm^{-3}
j_2 oxygen reaction current per unit volume of positive electrode, A cm^{-3}
j_3 cadmium reaction current per unit volume of the negative electrode, A cm^{-3}
j_4 oxygen reaction current per unit volume of negative electrode, A cm^{-3}
l total thickness of the cell unit, cm
l_1 half thickness of the nickel electrode, cm
l_2 thickness of the separator, cm
l_3 half thickness of the cadmium electrode, cm
l_y average thickness of active material in the nickel electrode, cm
L_{neg} loading in the cadmium electrode, g of $Cd(OH)_2/cm^3$ of void
M_i molecular weight of species i, g mol^{-1}
$P_{O_2,ref}$ reference oxygen pressure, atm
p a parameter
Q_{max} maximum theoretical charge in the nickel electrode, C cm^{-2} of electrode
Q amount of charge present in the nickel electrode at the end of charge or discharge operations, C cm^{-2} of electrode
R universal gas constant, 8.3143 J $mol^{-1}\ K^{-1}$
S_p^Q sensitivity coefficient of parameter p on the amount of charge Q present in the electrode at the end of a charge or discharge operation
S_p^V sensitivity coefficient of parameter p on the cell voltage V_{cell}, V
SOC state of charge defined in Eq. 74
SOD state of discharge defined in Eq. 73
T temperature, K
t time, s
t_-^o transference number of the anion OH^- with respect to the solvent velocity
$U_{i,ref}$ equilibrium potential for reaction i at reference conditions measured with respect to an Hg/HgO reference electrode, V
U_i^θ standard potential for reaction i, V
U_{RE}^θ standard potential for the Hg/HgO reaction in alkaline media, V
V_{cell} cell voltage defined in Eq. 75, V
x spatial distance from the center of the positive electrode, cm
y spatial distance from the nickel substrate surface, cm
y_o radius of the nickel substrate in cylindrical shape, cm

Greek

α_{ai} anodic transfer coefficient for reaction i
α_{ci} cathodic transfer coefficient for reaction i
β tortuosity factor associated to the porous solid material in the negative electrode
$\epsilon_{o,P}$ porosity of the nickel substrate in the positive electrode
$\epsilon_{o,N}$ porosity of the substrate in the negative electrode
ϵ_1 porosity of the positive electrode
ϵ_2 porosity of the separator with a 90% saturation level or wetability
ϵ_3 porosity of the negative electrode
$\epsilon_{3,max}$ porosity of the negative at fully charged state
$\epsilon_{3,min}$ porosity of the negative at fully discharged state
ϕ_1 potential in the solid phase, V
ϕ_2 potential in the liquid phase, V
ϕ_{sub} potential in the nickel substrate, V
γ_1 tortuosity factor associated with the porous positive electrode
γ_2 tortuosity factor associated with the porous separator
γ_3 tortuosity factor associated to the porous negative electrode
η_i overpotential for reaction i, V
κ electrolyte conductivity, S cm^{-1}
θ_N state of charge of the negative electrode
θ_P state of charge of the positive electrode
ρ_i density of species i, g cm^{-3}
σ_{Cd} conductivity of the solid material in the negative electrode, S cm^{-1}
σ_{Ni^*} conductivity of the active material in the positive electrode, S cm^{-1}
τ exponent for the local state of charge of the negative electrode included in the kinetic expressions defined in Eq. 42 and 43

REFERENCES

1. W. R. Scott and D. W. Rusta, *Sealed-Cell Nickel Cadmium Battery Applications Manual,* NASA Reference Publication 1052 (1979).
2. P. C. Milner and U. B. Thomas, in *Advances in Electrochemistry and Electrochemical Engineering,* P. Delahey and C. W. Tobias, Editors, Vol. 5, pp. 1-86, John Wiley and Sons, Inc., New York (1967).
3. H. B. Lunn and J. Parker, in *Proceedings of the 4th International Symposium on Research and Development in Non-Mechanical Electrical Power Sources,* D. H. Collins, Editor, pp. 129-145, Pergamon Press, Inc., New York (1964).
4. D. Fan and R. E. White, *This Journal,* **138,** 17 (1991).
5. D. Fan and R. E. White, *ibid.,* p. 2952.
6. K. W. Choi and N. P. Yao, in *Battery Design and Optimization,* S. Gross, Editor, PV 79-1, p. 62, The Electrochemical Society Proceedings Series, Princeton, NJ (1979).
7. P. J. Timmerman, S. Di Stefano, P. R. Glück, and D. E. Perrone, in *Proceedings of the 26th IECEC,* Vol. 3, p. 358, American Nuclear Society, La Grange Park, IL (1991).
8. D. M. MacArthur, *This Journal,* **117,** 729 (1970).
9. G. W. D. Briggs and P. R. Snodin, *Electrochim. Acta,* **27,** 565 (1982).
10. C. Zhang and S. Park, *This Journal,* **134,** 2966 (1987).

11. A. H. Zimmerman and P. K. Effa, *ibid.*, **131,** 709 (1984).
12. J. Bouet, F. Richard, and Ph. Blanchard, in *Nickel Hydroxide Electrodes,* D. A. Corrigan and A. H. Zimmerman, Editors, PV 90-4, p. 260, The Electrochemical Society Proceedings Series, Pennington, NJ (1990).
13. K. Micka and I. Rousar, *Electrochim. Acta,* **25,** 1085 (1980).
14. K. Micka and I. Rousar, *ibid.,* **27,** 765 (1982).
15. Z. Mao, P. De Vidts, R. E. White, and J. Newman, *This Journal,* **141,** 54 (1994).
16. J. S. Newman, *Electrochemical Systems,* 2nd ed., Prentice Hall, Englewood Cliffs, NJ (1991).
17. W. Tiedemann and J. Newman, *AIChE J.,* **21,** 25 (1975).
18. M. Sinha, PhD Thesis, University of California, Los Angeles (1982).
19. P. A. Antonenko, V. Z. Barsukov, N. G. Krapivnii, and L. N. Sagoyan, *Vopr. Khim. Khim. Teknol. (Kharkov),* **25,** 18, 135 (1972).
20. R. Barnard, C. F. Randell, and F. L. Tye, *J. Appl. Electrochem.,* **10,** 109 (1980).
21. *Handbook of Electrolyte Solutions,* Part A, V. M. M. Lobo, Editor, pp. 1073-1092, Elsevier, New York (1989).
22. S. G. Bratsch, *J. Phys. Chem. Ref. Data,* **18,** 1 (1989).
23. *CRC Handbook of Chemistry and Physics,* D. R. Lide, Editor, CRC Press, Inc., London, **12-36** (1992-93).
24. D. J. Downing, R. H. Gardner, and F. O. Hoffman, *Technometrics,* **27,** 151 (1985).
25. K. E. Gubbins and R. D. Walker Jr., *This Journal,* **112,** 469 (1965).

Doped $PrMnO_3$ Perovskite Oxide as a New Cathode of Solid Oxide Fuel Cells for Low Temperature Operation

Tatsumi Ishihara,* Takanari Kudo, Hideaki Matsuda, and Yusaku Takita

Department of Applied Chemistry, Faculty of Engineering, Oita University, Dannoharu 700, Oita 870-11, Japan

ABSTRACT

Cathodic overpotentials of $Ln_{0.6}Sr_{0.4}MnO_3$ (Ln = La, Pr, Nd, Sm, Gd, Yb, and Y) were studied for a new cathode of solid oxide fuel cell (SOFC). Cathodic overpotentials as well as the electrical conductivity strongly depended on the rare earth cations used for the A sites of perovskite oxide. Strontium doped $PrMnO_3$ exhibited the highest electrical conductivity among the examined perovskite oxide containing Mn for B sites. Moreover, overpotentials of Sr-doped $PrMnO_3$ cathode maintained low values in spite of decreasing the operating temperature. Consequently, almost the same power density of SOFC with $La_{0.6}Sr_{0.4}MnO_3$ cathode can be obtained at about 100 K lower operating temperature by using Sr-doped $PrMnO_3$ as the cathode. The overpotentials and electrical conductivity decreased and increased with increasing the amount of Sr dopant in $PrMnO_3$, respectively, and the lowest overpotential was attained at $x = 0.4$ in $Pr_{1-x}Sr_xMnO_3$. Comparing with $La_{0.6}Sr_{0.4}MnO_3$ oxide, the reactivity of $Pr_{0.6}Sr_{0.4}MnO_3$ with Y_2O_3-stabilized ZrO_2 is much less than that of $La_{0.6}Sr_{0.4}MnO_3$ and furthermore, the matching of thermal expansion of $Pr_{0.6}Sr_{0.4}MnO_3$ with Y_2O_3-ZrO_2 was satisfactorily high. Therefore, perovskite oxide of $Pr_{0.6}Sr_{0.4}MnO_3$ has a great possibility of the cathode materials for decreasing the operating temperature of solid oxide fuel cells.

Introduction

Solid oxide fuel cell (SOFC) is a new electric power generation system with less emission of pollutant, low noise, and high energy conversion efficiency. In particular, it is reported that the energy conversion efficiency is attained as high as 90% by combining with the heat recovery and steam turbine system. Furthermore, the steam reforming of fuels such as methane can directly proceed on the anode of SOFC, since the operating temperature is high. Decreases in the cost per unit electric power generated and the enhancement of reliability as a generation system are the current subjects for the practical application of SOFC. Although the operation of SOFC is generally studied at 1273 K, [1] the advantages of SOFC listed are obtained by operating the temperature above 973 K and moreover, refractory metal alloys can be used for cell stacking by decreasing the operating temperature of SOFC down to 973 K. Therefore, the decreases in the operating temperature of SOFC without decreases in the power density make it possible to eliminate the problems of cost and reliability in SOFC system. However, the rate of chemical reaction at the electrode decreases remarkably with decreasing operating temperature, and consequently, the overpotential of electrode becomes the main cause for the voltage drops of cell when the cell is operated in the low temperature range. On the other hand, the apparent activation energy of the $La_{0.6}Sr_{0.4}MnO_3$ cathode which was estimated from the temperature dependence of overpotential is 74 kJ/mol, which is larger than that of Ni anode, 64 kJ/mol. Therefore, it is expected that the decreases in the voltage drops due to the overpotentials of electrode, particularly, cathode are of importance for decreasing the operating temperature of SOFC without decreasing the power density. Perovskite type oxides of Sr-doped $LaMO_3$ (M = Mn, Co, Cu, Fe) have been studied as cathode materials; [2-4] however, these cathode oxides except for doped $LaCoO_3$ were examined at the operating temperature of 1273 K. The doped $LaCoO_3$ oxide is studied as a cathode material for SOFC operating at intermediate temperature, [4] while there are many difficulties for the application of $LaCoO_3$ for the cathode of SOFC. [1] On the other hand, almost all studies on cathode materials use La^{3+} cations for the A site element in perovskite oxide, ABO_3. In our previous study, we investigated the effects of rare earth cations in the A site upon the cathodic overpotential of perovskite-type oxide containing Mn for B site cations, and it was found that A site cations have a great influence on the cathodic property of perovskite oxide. [6] In the present study, the effects of A site cations as well as the dopant for A site on the cathodic property were studied in further detail for the development of a new cathode with low overpotential in a low temperature region. The thermal expansion property and the reactivity of $PrMnO_3$ with YSZ electrolyte were also studied.

Experimental

Perovskite-type oxide of $Ln_{0.6}Sr_{0.4}MnO_3$ (Ln = La, Pr, Nd, Sm, Gd, Yb, and Y) was prepared by the evaporation to dryness of the calculated amount of aqueous solutions of commercial Ln_2O_3 (99.99% pure), $Sr(NO_3)_2$, and $Mn(CH_3COO)_2$. The consequently obtained powders were calcined at 1473 K for 3 h and then applied to one face of YSZ disk (5 mm in diameter) as a cathode. YSZ disks

* Electrochemical Society Active Member.